

# Graphene-Based Flexible and Eco-Friendly Wearable Electronics and Humidity Sensors

Filipe L. J. Diniz<sup>a</sup> , Thaíses B. S. Lima<sup>a</sup> , Elmo S. Araujo<sup>a</sup> , Patricia L. B. Araujo<sup>b\*</sup> 

<sup>a</sup>Universidade Federal de Pernambuco (UFPE), Departamento de Energia Nuclear, Av. Prof. Luiz Freire, 1000, Cidade Universitária, 50740-545, Recife, PE, Brasil.

<sup>b</sup>Universidade Federal de Pernambuco (UFPE), Departamento de Engenharia Biomédica, Av. Jornalista Anibal Fernandes, Cidade Universitária, 50740-560, Recife, PE, Brasil.

Received: November 04, 2023; Revised: January 09, 2024; Accepted: February 20, 2024

A novel, efficient, and cost-effective coating method was developed for fabricating highly conductive cotton yarn loaded with reduced graphene oxide (rGO). This method is straightforward, rapid, scalable, and amenable to solution processing. The key innovation involves pretreating the cotton yarn with chicken egg albumin (CEA) before applying the rGO coating through a simple dip-and-dry process. This method significantly reduces the electrical resistance of the cotton yarn, achieving an optimal specific resistance of 80  $\Omega \cdot \text{g}/\text{cm}^2$  with just five coating cycles. Additionally, the coated samples exhibit exceptional reliability, enduring  $10^4$  bending tests and 5 washing tests without compromising conductivity. Notably, the study reveals consistent proportional variations in response to changes in relative humidity, regardless of the initial reference resistance value or yarn characteristics. These stable and conductive rGO-coated cotton yarns (rGO CY) might be seamlessly integrated into textiles and garments, enabling the development of flexible and wearable electronics, as well as sensors.

**Keywords:** Cotton yarn flexible sensors, chicken egg albumen, dip and dry coating, reduced graphene oxide, humidity sensor.

## 1. Introduction

Natural fibers coated with graphene-based materials have gained significant attention for their application in flexible and wearable electronic fibers (e-fibers) owing to their environmentally friendly nature, cost-effectiveness, and abundant renewable resources<sup>1</sup>. Graphene, an allotrope of carbon, represents the thinnest possible atomically flat layer, consisting of a monolayer of carbon atoms arranged in a honeycomb planar hexagonal network held together by strong C—C bonds<sup>2</sup>. The unique structure of graphene imparts extraordinary properties such as high electrical conductivity (up to 200  $\text{cm}^2 \cdot \text{V}^{-1} \cdot \text{s}^{-1}$ )<sup>3</sup>, high thermal conductivity (5300  $\text{W} \cdot \text{m}^{-1} \cdot \text{K}^{-1}$ )<sup>4</sup>, impressive strength, lightweight structure, and large surface area (2630  $\text{m}^2 \cdot \text{g}^{-1}$ )<sup>5</sup>, which have attracted significant attention in the field of nanotechnology. However, the weak van der Waals forces that hold the graphene layers stacked on graphite are insufficient to establish a stable adhesive bond between graphene and the surface of cotton yarn.

Koçanalı and Apaydın Varol<sup>6</sup> reported the requirement of 90 coating cycles to decrease the surface resistivity of reduced graphene oxide (rGO) coated yarns from 90 M $\Omega$  to 8.18 k $\Omega$  using a simple dip-coating process, without a binder, through the dip-and-dry method. Previous studies attempted to enhance the effectiveness of dip-and-dry cycles by utilizing organic and inorganic synthetic binding agents such as dopamine<sup>7</sup>, polyvinylpyrrolidone<sup>8-10</sup>, polyethyleneimine<sup>10</sup>,

Polyvinyl alcohol<sup>11</sup>, polypyrrole<sup>12</sup>, 3-glycidioxypropyl trimethoxy silane<sup>13</sup>. With the aid of these coupling agents, graphene oxide (GO) or rGO was successfully coated onto textiles with an average of 10 dip-and-dry cycles. Other researchers have employed biomolecules, such as bovine serum albumin (BSA)<sup>14-16</sup>, as a wrapping method to improve the electrostatic self-assembly between GO and various yarn types. However, many of these coupling agents such as BSA, are expensive to procure, and some pose challenges in synthesis. Moreover, additional steps of removing binding agents from the fabrics were applied after the loading process, further increasing the time and cost involved<sup>6</sup>.

Among different natural organic materials, chicken egg albumin (CEA) stands out as a promising candidate for enhancing the surface adhesion between cotton yarns and graphene derivatives. Despite being a biomolecule like BSA, CEA is more affordable, and fabricating flexible devices using CEA is simpler when compared to those utilizing BSA. The extraction process of proteins like BSA from bovine blood is complex, expensive, slow, involves multiple stages, and is time-consuming, resulting in high production costs and challenges in accessing a steady supply of bovine blood<sup>17-19</sup>. These limitations hinder large-scale production of expensive proteins in laboratories. In contrast, CEA is easily obtained from eggs<sup>20</sup>, presenting a more accessible alternative. Furthermore, due to its biodegradability, bioresorbability, eco-friendliness, and mechanical flexibility, CEA is considered one of the most suitable materials for next-generation wearable and bio-devices<sup>21</sup>.

\*e-mail: [patricia.lbaraujo@ufpe.br](mailto:patricia.lbaraujo@ufpe.br)

In the context of humidity sensors, after thermal reduction, electrical insulating GO is converted into conductive rGO, with its conductivity being sensitive to water molecules due to the defects and remnant reactive oxygen functional groups<sup>22</sup>. However, the bonding between the rGO film and the substrate is usually weak. In this work, CEA was used as an adhesive for fabricating rGO-coated cotton yarns (rGOCY) for conductive wires and humidity sensing. It was observed that the electrical resistance of rGOCY increases linearly as the relative humidity (RH) increases within the range of 11% RH to 90% RH, with an excellent correlation coefficient of 0.99. Furthermore, it was found that proportional variations occur for the same changes in relative humidity, regardless of the initial value of the resistance and the characteristics of rGOCY. It was possible to extract a calibration curve from this behavior profile that can be used to calibrate any rGOCY pre-treated with CEA. This calibration methodology is important because it eliminates the need to perform calibration curves with several different humidity levels. All yarns behave the same way; it is only necessary to know the resistance of rGOCY at a specific humidity. By applying this value in a general calibration equation, rGOCY works as a calibrated humidity sensor.

Based on the aforementioned information, we have adopted an environmentally friendly coating process to fabricate wearable cotton yarns coated with rGO. We utilized a simple and unique dip-and-dry coating technique to apply thermally rGO sheets to cotton yarns. This approach provides a cost-effective method with potential for producing highly conductive textiles. Furthermore, we investigated the usability of these coated yarns as humidity sensors, further expanding their application scope.

## 2. Experimental Section

### 2.1. Materials

Cotton yarn (TEX – 164) purchased from the local cloth market. Eggs were purchased from the supermarket. Intercalated graphite flakes were purchased from Sigma Aldrich. Barium chloride ( $\text{BaCl}_2$ ) and absolute ethanol were purchased from Cinética Química (Brazil). Sodium hydroxide (NaOH), calcium nitrate tetrahydrate ( $\text{Ca}(\text{NO}_3)_2 \cdot 4\text{H}_2\text{O}$ ), and sodium chloride (NaCl) were purchased from Dinâmica Química (Brazil). Magnesium chloride hexahydrate ( $\text{MgCl}_2 \cdot 6\text{H}_2\text{O}$ ) was purchased from Neon. All reagents were of analytical grade and were used as supplied.

### 2.2. Methods

#### 2.2.1. Preparation of reduced graphene oxide (rGO)

GO was obtained from intercalated graphite flakes using Hummer's chemical oxidation method<sup>23</sup>. Various methods can be employed to reduce GO to rGO, such as chemical, thermal, photocatalytic, and electrochemical approaches. In this study, we employed the thermal reduction method described by Oliveira et al.<sup>24</sup>. Dry GO powder was placed in a porcelain crucible and introduced into a preheated muffle furnace, undergoing thermal treatment at 350°C for 30 seconds. It's crucial to slowly remove the crucible from

the furnace to prevent material loss, as a pressure difference could disperse the material in the air. The resultant product was a black powder of thermally rGO.

#### 2.2.2. Chicken egg albumin separation

Egg products, especially albumin, serve as significant protein sources for creating films and coatings<sup>25</sup>. Typically, CEA can be easily obtained from eggs without any synthesis or extraction. The process involves separating egg white from the yolk, followed by pre-treatment steps such as dilution in water, homogenization, and filtration to obtain the raw material for separation<sup>26</sup>. In this study, our approach aligns with previous methodologies<sup>21,27</sup>, utilizing CEA without purification, showcasing its straightforward utilization.

Initially, egg white (EW) was extracted from a randomly selected fresh chicken egg obtained from the market and utilized as a functional adhesive for adhesion of rGO onto cotton yarns. The separation of EW from the egg yolk was conducted in a clean laboratory environment using a stainless-steel mesh spoon. Subsequently, the isolated EW was gathered in a becker and blended with deionized water (DW) at a 1:1 volume ratio employing a pipette. The EW solution underwent sonication for 10 minutes (at 20% amplitude) using an immersion ultrasonic probe (Sonic Vibra Cell Vc505, 500W, 20kHz, Sonics & Materials) at room temperature. The resultant mixture was then filtered to eliminate any solid particles. Subsequently, it was dried in an oven at 60°C for 48 hours. After the drying process, the residual material was mechanically crushed and sieved to obtain a fine powder of CEA. To mitigate the risk of protein degradation, the CEA powder was kept dry and refrigerated, only rehydrating it immediately before use.

#### 2.2.3. Preparation of reduced graphene oxide coated yarns (rGOCY)

In this study, cotton yarns were employed for impregnation with rGO. Initially, the yarn was washed with acetone and distilled water to eliminate impurities, then dried in an oven at 60°C for 24 hours. To enhance rGO adhesion, the cotton yarn underwent functionalization with CEA. The yarns were immersed in a previously ultrasonicated solution of deionized water and 0.5% CEA powder by weight, using an immersion ultrasonic probe at 20% amplitude at room temperature for 10 minutes, and gently stirred for 30 minutes at room temperature. Subsequently, the CEA-coated yarns were dried under an exhaust hood for 2 hours.

CEA-coated yarns were further coated with rGO using the dip-and-dry method<sup>6</sup>. The aqueous solution of the nanocomposite used during the immersion and drying cycles was prepared as follows: 100 mg of rGO powder was mixed with 20 mL of 70% ethanol and sonicated for 10 minutes. The cotton yarn was gently immersed in the aqueous solution for 10 minutes with mild stirring to allow for the electrostatic self-assembly of rGO onto the surfaces of the CEA-coated yarn fibers, and then promptly dried in an oven at 80°C. All cycles were completed in the same manner. Figure 1 illustrates the preparation method of rGO-decorated cotton yarns. The cotton yarn not coated with rGO and the rGOCY, was weighed to calculate the coating ratio using the following Equation 1<sup>6</sup>:

$$\text{Coating Ratio (CR)} = \frac{w_f - w_c}{w_c} \times 100 \quad (1)$$

where  $w_f$  is the weight of the coated yarn after the completion of the coating cycles, and  $w_c$  is the weight of the cotton yarn before the coating process.

### 2.3. Characterization

#### 2.3.1. X-ray diffraction (XRD) measurements.

Diffractograms for the GO and rGO were obtained using the Rigaku SmartLab® X-ray diffractometer, equipped with a high-flux 9 kW rotating anode PhotonMax X-ray source coupled to a high-resolution energy-dispersive 2D semiconductor detector, HyPix-3000. Data were collected in the range of  $5^\circ$  to  $90^\circ$  with a step size of  $0.01^\circ$  and an acquisition speed of  $3^\circ/\text{min}$ .

#### 2.3.2. Fourier transform infrared (FTIR) spectroscopy.

GO and rGO were analyzed through Fourier Transform Infrared (FTIR) Spectroscopy in a FTIR-4600, JASCO-Japan, equipped with an Attenuated Total Reflection accessory ATR ProOne (ZnSe Crystal). Experiments were performed with 32 scans,  $4 \text{ cm}^{-1}$ , in the  $4000 - 500 \text{ cm}^{-1}$  wavenumber range.

#### 2.3.3. Scanning electron microscopy (SEM) analysis

Scanning electron microscopy (SEM) experiments were performed using the TESCAN MIRA3 FEG-SEM model equipment, with an acceleration voltage of 20 kV and magnification up to 200,000x, on rGO-coated samples.

#### 2.3.4. Resistivity measurement of rGOCY.

Electrical resistances of rGOCY samples were measured using a two-probe Fluke 83 III multimeter. rGOCY resistance measurements were performed in incremental separations of 1 cm intervals from 1 to 5 cm, and the average electrical resistance,  $R$ , of the recorded measurements, was obtained. It is more convenient to express the electrical resistance in terms of mass-specific resistance,  $R_m$ , for yarns and textile fibers<sup>28</sup>. According to the definition, the mass-specific resistance ( $R_m$ ) in  $\Omega \cdot \text{g}/\text{cm}^2$  is connected to the specific resistance ( $\rho$ ) usually expressed in  $\Omega \cdot \text{cm}$  through the following relationship expressed in the Equation 2:

$$R_m = \rho d \quad (2)$$

where  $d$  is the density of material in  $\text{g}/\text{cm}^3$ .

However, when dealing with textile fibers or yarns, it is more advantageous to express the mass-specific resistance,  $R_m$ , about the linear density of the fiber or yarn.

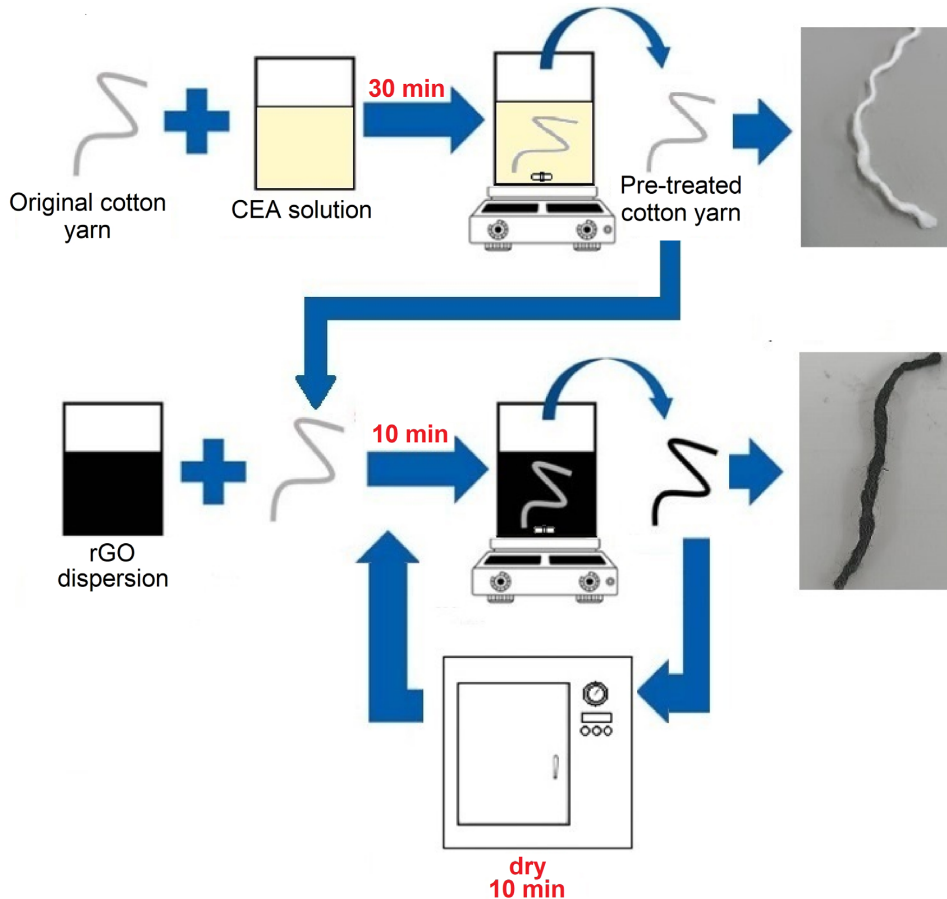


**Figure 1.** Pre-treatment method of cotton yarns with CEA and subsequent decoration with rGO using the dipping and drying method.

Therefore, the mass-specific resistance,  $R_m$ , in  $\Omega \cdot \text{g}/\text{cm}^2$  of an arbitrary sample is given by Equation 3:

$$R_m = \frac{RNT}{l} \quad (3)$$

where  $R$  is the resistance in  $\Omega$ ,  $l$  is the distance between the ends of the specimen (cm),  $N$  is the number of ends of the yarn or fiber, and  $T$  is the linear density of the textile yarn or fiber (g/cm).

### 2.3.5. Durability testing for bending cycles and washing cycles

As the invariance in the electrical conductivity of e-textiles under various conditions is crucial for wearable and flexible electronics, we measured the cycle-dependent resistivity of rGOCY under bending/flexing and washing. To demonstrate the wire stability against bending, the bending tests were conducted in 1 cm-sized rGOCY into a chamber with controlled temperature and humidity, using a custom-made two-point bending device and a mechanical system coupled to an automatized recording log, as shown in Figure 2. The durability of the electrical resistivity values concerning washing cycles was evaluated using a beaker containing distilled water. rGOCY samples were placed under magnetic stirring at 300 rpm for 10 minutes. Electrical resistivity was measured after each washing cycle.

### 2.3.6. Relative humidity test environment

To investigate the correlation between the electrical resistance of rGOCY and relative humidity, we conducted measurements of current versus voltage (I-V) characteristic curves (KEITHLEY 6517B Electrometer) for wire samples under several controlled relative air humidity conditions using saturated aqueous solutions of inorganic salts commonly employed for calibrating humidity sensors<sup>29</sup>.

Hence, in order to achieve the required environmental conditions, we placed saturated solutions of lithium chloride (LiCl), calcium nitrate ( $\text{Ca}(\text{NO}_3)_2$ ), magnesium chloride ( $\text{MgCl}_2$ ), sodium hydroxide (NaOH), sodium chloride (NaCl), or barium chloride ( $\text{BaCl}_2$ ) in sealed containers at a constant temperature of 24°C. To achieve stable relative humidity values, as shown in Table 1.

The humidity detection performance was evaluated by placing the sensor inside a chamber where water vapor ( $\text{H}_2\text{O}$ ) was introduced and analyzing the change in electrical resistance concerning the variation in relative humidity within the chamber. The humidity levels were controlled using a flow valve. To measure the resistance change, we employed an Arduino Nano board along with a commercial humidity and temperature sensor (AHT20) to monitor the relative humidity in the gas exposure chamber. The equipment encompasses the following subsystems: a gas distribution system, a bubbler, and a gas exposure chamber. All these components are managed by a personal computer using integrated programs equipped with user-friendly graphical interfaces (Matlab), as illustrated in Figure 3.

**Table 1.** Relative humidity in different saturated salt solutions.

Saturated salt solution (24°C)	Relative humidity (% RH)
LiCl	11
$\text{MgCl}_2$	33
$\text{Ca}(\text{NO}_3)_2$	51
NaCl	75
$\text{BaCl}_2$	90

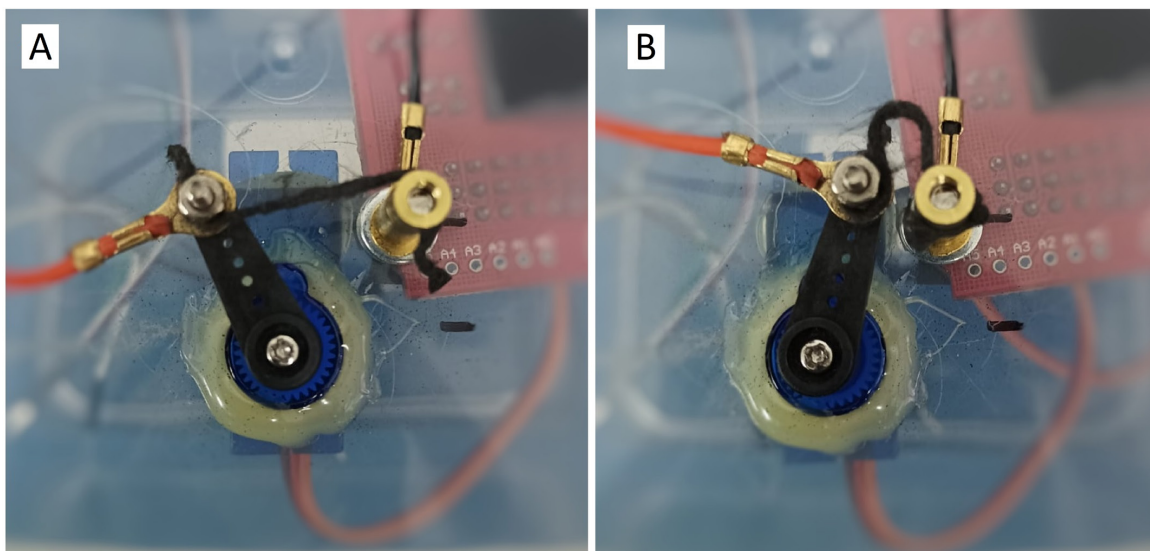


**Figure 2.** Bending test in two states: (A) stretched yarn; (B) folded yarn.

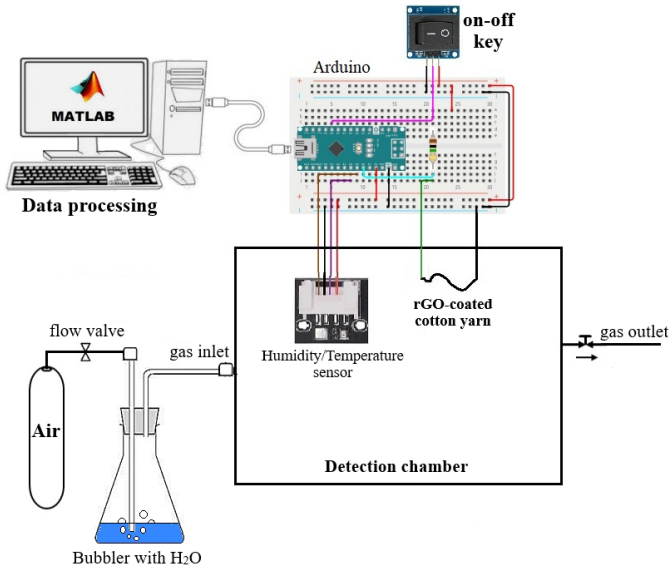


**Figure 3.** Experimental setup for humidity detection.

### 3. Results and Discussion

#### 3.1. X-Ray diffraction (XRD) analysis

To investigate the successful formation of graphene oxide (GO) and thermally reduced graphene oxide (rGO) and to track changes in interplanar spacing and the presence of functional groups, X-ray diffraction (XRD) analysis was performed. Figure 4 shows the XRD patterns for pristine graphite flakes, GO, and rGO. A prominent diffraction peak (002) with high intensity at  $2\theta = 26.5^\circ$ , corresponding to the interplanar spacing ( $d_{002}$ ) of graphite ranging from 334.8 to 336 nm is observed<sup>30</sup>. In the case of GO, a greater peak appears at  $12.01^\circ$ , indicating an expansion in the layer spacing due to the presence of intercalated water molecules and various functional groups resulting from the oxidation of graphite<sup>31</sup>. These findings are consistent with previous reports on GO solids<sup>30,31</sup>. After thermal reduction treatment, rGO exhibits a diffraction peak (002) at  $2\theta = 23.62^\circ$ , similar to that of graphite. This shift in the peak position is attributed to the removal of intercalated water molecules and oxide groups from the surface of GO<sup>31</sup>.

#### 3.2. FTIR analysis

The presence of functional groups in graphite, graphene oxide (GO), and reduced graphene oxide (rGO) samples was determined using FT-IR spectroscopy. The results obtained from FTIR-ATR characterization, depicted in Figure 5, show the expected absence of prominent peaks in the FTIR spectra of graphite due to its chemical inertness<sup>32</sup>. However, in the GO spectrum, a series of distinctive bands associated with stretching and bending modes confirm the oxidation of graphene during the oxidation process of graphite. The main observed bands are as follows: a broad band centered at  $3336\text{ cm}^{-1}$ , which corresponds to the stretching vibrations of the O–H groups present in carboxyl, alcohol, and absorbed water molecules, respectively<sup>32</sup>.

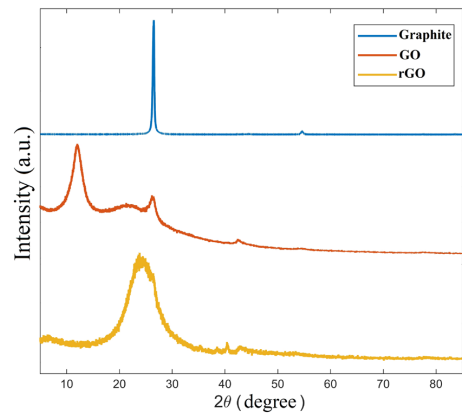


**Figure 4.** X-ray diffraction patterns of pristine graphite, graphene oxide (GO), and reduced graphene oxide (rGO).

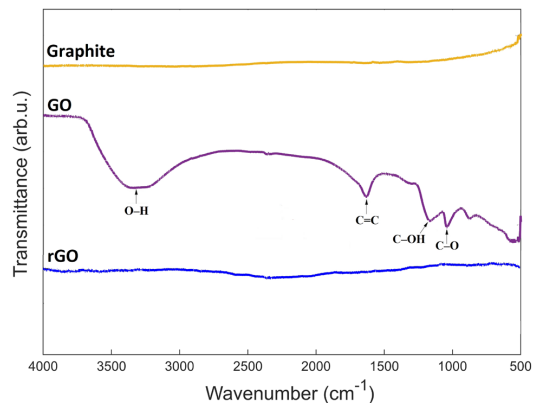


**Figure 5.** FTIR spectra of Graphite, graphene oxide (GO), and thermally reduced graphene oxide (rGO).

Additionally, the stretching of the C–OH group is present at  $1226\text{ cm}^{-1}$ <sup>34</sup>. Another important band is observed at  $1630\text{ cm}^{-1}$ , which signifies the in-plane stretching of the  $\text{sp}^2$  hybridized carbon atoms (C=C) in the graphene structure<sup>33</sup>; Furthermore, bands at  $1164\text{ cm}^{-1}$  and  $1043\text{ cm}^{-1}$  are assigned to the C–O from carbonyl, carboxylic, and epoxy groups<sup>32-34</sup>. These findings strongly support the occurrence of effective chemical oxidation in the process of converting graphite to graphene oxide. Following the thermal treatment, no evidence of absorption bands related to functional groups, such as OH, epoxy, C–O, and C=O derived from COOH groups, is observed, successfully confirming the reduction of GO to rGO.

### 3.3. Morphological analysis of rGOCY

The morphological characteristics of the cotton yarn decorated with rGO were investigated through SEM analysis.

SEM images in Figure 6A and 6B depict the cotton yarn coated with CEA as a pre-treatment and the cotton yarn coated with rGO, respectively. CEA-coated yarn coated exhibits a clean and smooth surface. Upon applying the rGO coating treatment, the surface becomes rough. With an increase in rGO loading, the pores or voids within the yarn gradually fill with rGO. The color of the yarn changed after each dip-coating treatment. However, following the application of rGO, an aggregation of rGO flakes on the surface becomes evident, accompanied by fiber condensation and the accumulation of rGO layers. Upon zooming in on the image (at 7690x magnification) using SEM, the development of wrinkles, undulations, and edges of the rGO sheets on the coated yarn surface can be observed. These observations clearly indicate the formation of a bond between the cotton and rGO, as highlighted in Figure 6C and 6D.

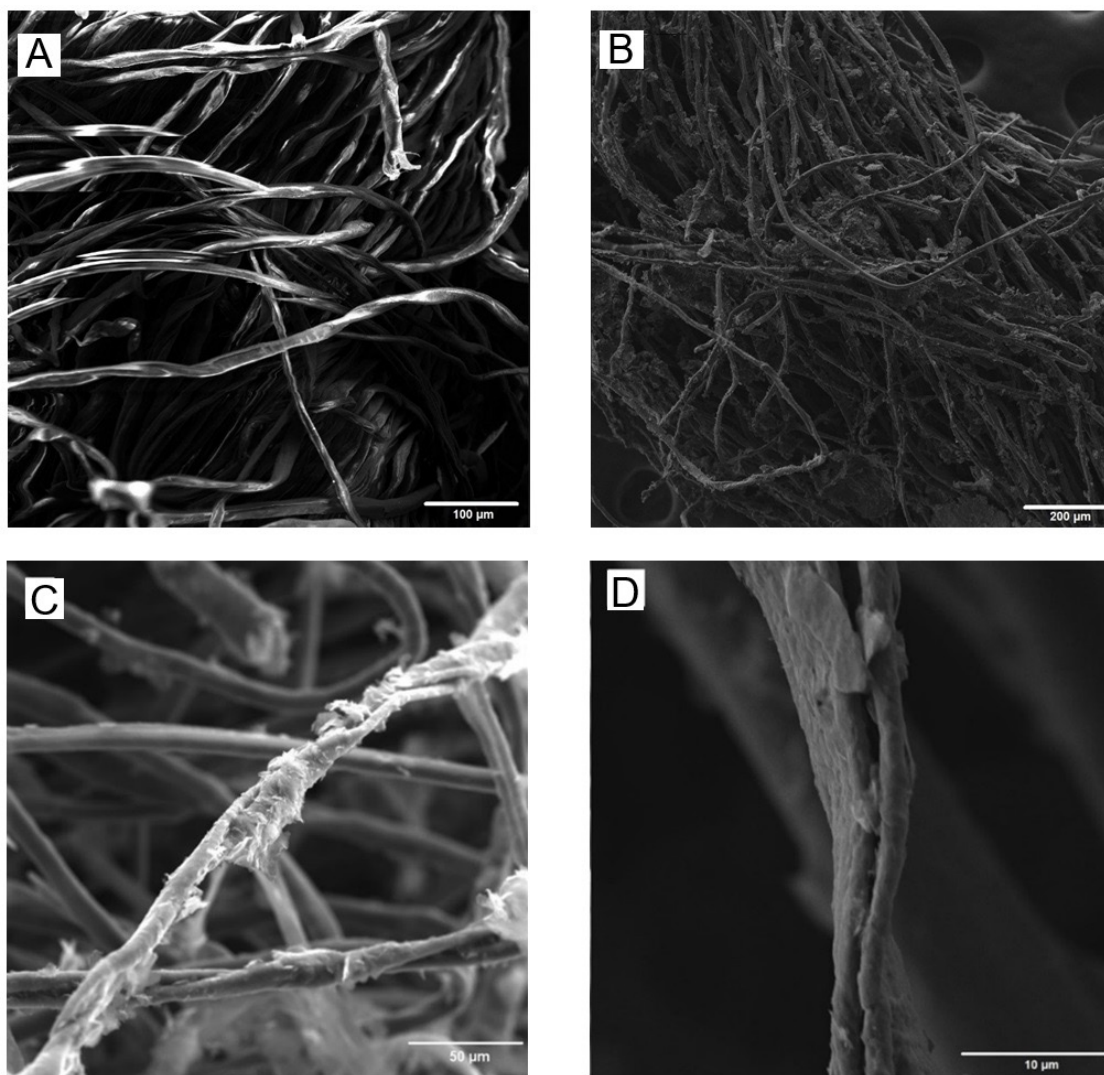


**Figure 6.** SEM of cotton yarn samples: (A) treated with CEA; (B) covered with rGO; (C) and (D) cotton yarn samples coated with rGO (at 7690x magnification).

### 3.4. Effects of dip-coating cycles on electrical properties

Yarn electrical surface resistivity was measured using the two-probe method<sup>35</sup>, and the effect of dip-coating cycles on resistance is shown in Figure 7A. Untreated cotton yarns are considered insulators since the specific resistance of uncoated cotton fibers exceeded the measurable range of the ohmmeter. However, according to the literature<sup>28</sup>, the mass-specific resistance of cotton fibers at 65% relative humidity is  $10^{6.8} \Omega \cdot \text{g}/\text{cm}^2$ . A decrease in resistivity was observed during initial dip-coating cycles with rGO coating. Mass-specific resistance ( $R_m$ ) of the coated fibers gradually decreases as the dip-coating cycles are repeated at room temperature, a behavior compatible with previous studies<sup>9,10</sup>.

This phenomenon can be attributed to the accumulation of more material on the fiber, forming a continuous conductive network throughout the yarn, resulting in high electrical conductivity<sup>36</sup>. From the 5th immersion coating cycle onwards, the specific resistance is  $80 \pm 7 \Omega \cdot \text{g}/\text{cm}^2$ , with no significant further changes in  $R_m$  values. Moreover, when we connected the rGOCY, the LEDs lit up (Figure 7A inset). The brightness of the LED lights increased with the number of dip-coating cycles. As shown in Figure 7B, the coating performance improves rapidly in the initial cycles; however, after 6 cycles, the rate of increase decelerates due to the reduction in the number of CEA binding sites available on the cotton yarn and the agglomeration of rGO flakes on the surface, which is in line with previous observations<sup>6</sup>.

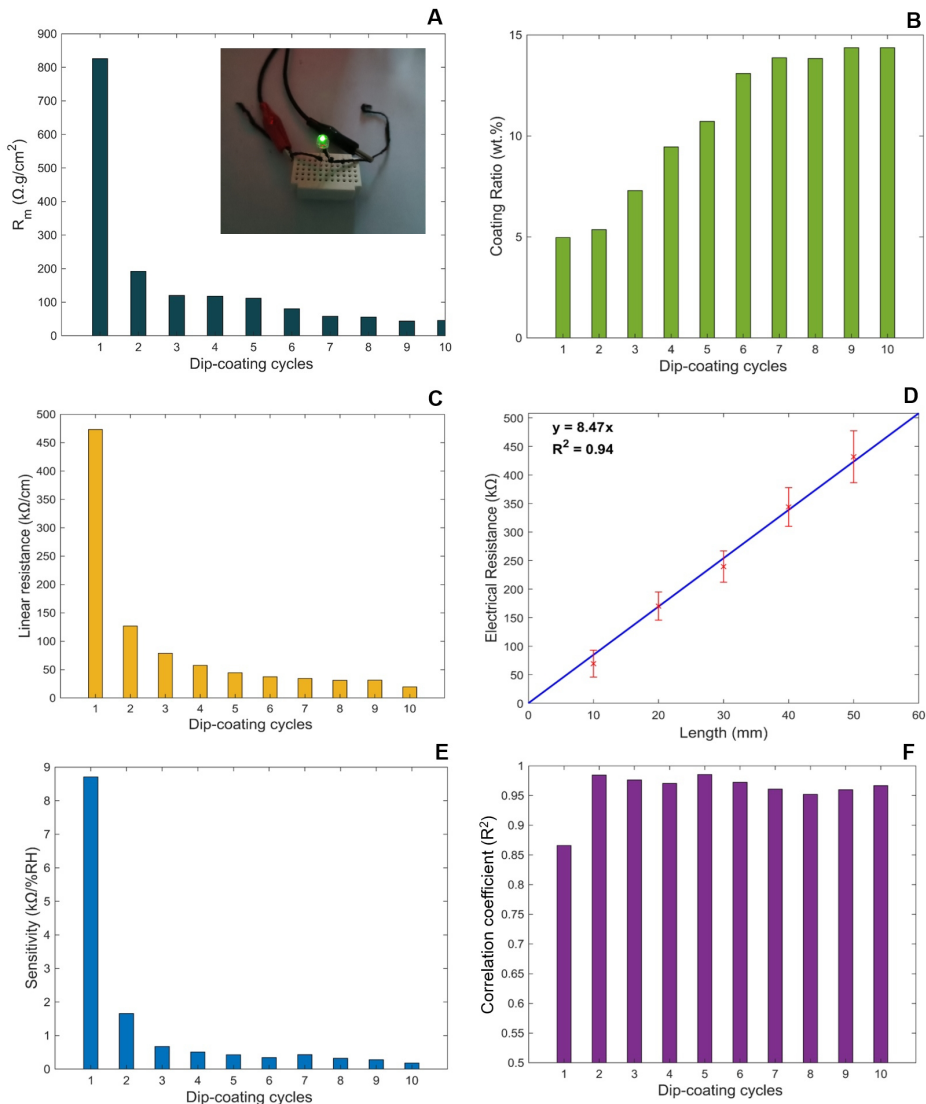


**Figure 7.** (A) Mass-specific resistance ( $R_m$ ) of the rGOCY varying the dip-coating cycles; (B) rGO coating ratio on cotton yarn as a function of dip-coating cycles; (C) Linear resistance ( $\text{k}\Omega/\text{cm}$ ) of rGOCY as a function of dip-coating cycles; (D) Electrical resistance along yarn length for rGOCY after 3 dip-coating cycles; (E) Sensitivity ( $\text{k}\Omega/\%RH$ ) of cotton yarns coated with rGO as a function of dip-coating cycles; (F) Correlation coefficient of rGOCY's humidity sensitivity as a function of dip-coating cycles.

In Figure 7C, a graph illustrates the linear resistance ( $k\Omega/cm$ ) of cotton yarns coated with rGO as a function of dip-coating cycles. Notably, the linear resistance experiences a sharp decline from the first to the second dip-coating cycle, after which it stabilizes starting from the fourth dip-coating cycle, with no significant further alterations observed. This information is crucial because stability in linear resistance across different coating cycles is essential to ensure the reliability of electronic devices. When linear resistance stabilizes after a certain number of coating cycles, as observed in the graph (Figure 7C), it indicates that the coating process has reached a state where the amount of deposited conductive material is consistent and predictable. The electrical resistance (in  $k\Omega$ ) of the cotton yarn against the sample length (in mm) is shown in Figure 7D. The resulting resistance is highly linearly correlated with the sample length ( $R^2 = 0.94$ ). These results indicate that the yarns coated with rGO are uniformly coated along the yarns and between different sections of the yarn, consistent with the reported findings in previous studies<sup>37</sup>. The slope of these linear graphs represents the resistivity of the yarns in  $k\Omega/mm$ , determined as 8.47 for the cotton yarn coated with rGO with only 3 dip-coating cycles. The detailed comparison of the electrical performance of rGOCY, pre-treated with CEA, and various other reported rGO-coated cotton e-textiles using the dip-coating method, along with the corresponding number of dip-coating cycles, is presented in Table 2.

In order to investigate the linearity and sensitivity properties of rGO-based conductive cotton yarn as a humidity sensor, the sensitivity of the sample was examined about the number of dip-coating cycles, as depicted in Figure 7E and 7F.

With an increase in the number of cycles, the sensitivity of the conductive yarn sample decreased, stabilizing after only four dip-coating cycles reaching a saturation point where the resistance of the yarn remained unchanged from one coating cycle to the next. In contrast, its correlation coefficient demonstrated a significant linearity improvement with just two dip-coating cycles and remained nearly constant around 0.98 thereafter. For this study, the optimal number of dip-coating cycles was determined to be three. This choice best aligned with all pertinent parameters, encompassing specific resistance ( $120.3 \Omega \cdot g/cm^2$ ), linear resistance ( $84.7 k\Omega/cm$ ), coating ratio (7.2%), humidity sensitivity ( $0.68 k\Omega/\% RH$ ), and the correlation coefficient response dependence (0.98) between resistance and relative humidity.

### 3.5. Mechanical flexibility and electrical stability of rGOCYs

Mechanical flexibility is a crucial factor affecting the reliability and durability of electronic devices used in flexible electronics applications. The electrical resistance of the rGOCY sample was measured during repetitive cycles of bending and stretching. As shown in Figure 8A, the variation in the electrical resistance of the rGOCY was marginal over 10000 bending cycles, which is comparable with the reported value in previous studies<sup>41,42,46</sup>. Furthermore, there was minimal difference between the resistance of folded and stretched yarns, which remained nearly constant throughout the bending cycles. These results indicate that rGOCY exhibits excellent mechanical properties, providing enhanced durability and reliability to flexible electronic devices.

**Table 2.** Electrical performance comparison of rGO-coated cotton e-textiles fabricated by dip-coating method using different pre-treatment or coupling agents and number of dip-coating cycles.

Substrate type	Reduction method	Component responsible for conductivity	Resistivity	Cotton pre-treatment or coupling agent	N° of dip-coating cycles	Ref.
Fabric	Heat treatment	rGO- PPy	0.83 $\Omega \cdot cm$	-	1	Xu et al. <sup>38</sup>
Yarn	HI acid	rGO	0.081 $\Omega \cdot cm$	BSA	1	Yun et al. <sup>14</sup>
Fabric	$NaBH_4$	rGO	8.18 $k\Omega/m^2$	-	90	Koçanalı and Apaydın Varol <sup>6</sup>
Yarn	Hydrazine	rGO-ZnO NNs	0.59 $\Omega \cdot cm$	APTES	1	Li et al. <sup>39</sup>
Fabric	Heat treatment	rGO	33.3 $\Omega \cdot sq^{-1}$	Air plasma	3	Wu et al. <sup>40</sup>
Yarn	Hydrazine	Functionalized rGO	4.2 $k\Omega/cm$	PEI	20	Kim et al. <sup>10</sup>
Fabric	$Na_2S_2O_4$	rGO-AgNP rGO-CuNP	6.42 $k\Omega/sq$	GLYMO	3	Bhattacharjee et al. <sup>13</sup>
Yarn	HI acid	rGO-AuNP	0.0035 $\Omega \cdot cm$	BSA	1	Yun et al. <sup>41</sup>
Fabric	$NaBH_4$	rGO	49.74 $k\Omega$	PEI and casein	10	An et al. <sup>27</sup>
Yarn	Hydrothermal	rGO- $TiO_2$	3.6 $K\Omega/sq$	-	1	Karimi et al. <sup>8</sup>
Yarn	HI acid and $C_2H_3NaO_2$	rGO	1 $\Omega \cdot cm$	Mercerization	1	Yun et al. <sup>42</sup>
Fabric	Hydrazine	rGO-AgNP	0.59 $\Omega \cdot cm$	PVP	30	Ghosh et al. <sup>9</sup>
Fabric	Heat treatment	rGO	290 $M\Omega/sq$	Organosilicon/ Noctylamine	4	Mizerska et al. <sup>43</sup>
Fabric	Hydrazine	rGO- PPy	7.5 $\Omega \cdot sq^{-1}$	-	12	Yaghoubidoust et al. <sup>12</sup>
Fabric	$NaBH_4$	rGO	560 $\Omega \cdot sq^{-1}$	-	20	Xu et al. <sup>44</sup>
Fabric	Heat treatment	rGO	10 <sup>4</sup> $\Omega/m^2$	-	3	Cai et al. <sup>45</sup>
Yarn	Heat treatment	rGo	80 $\Omega \cdot g/cm^2$	CEA	5	This work

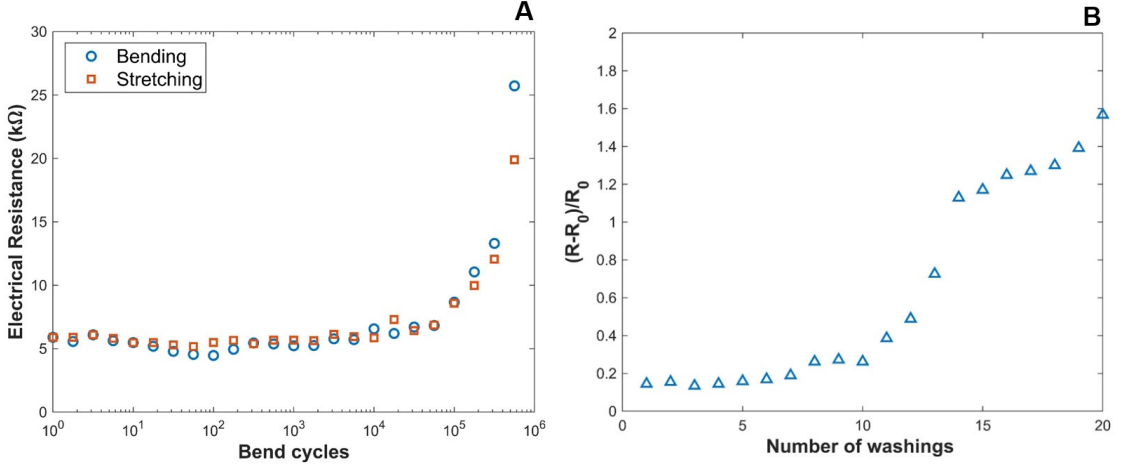


**Figure 8.** (A) Electrical resistance stability during bending cycles; (B) Effect of washing cycles on electrical resistance.

For a more precise analysis of the influence of washing cycles on the electrical resistance of rGOCY, we adopted the percentage variation in resistance  $((R - R_0) / R_0)$  as the analysis factor, where  $R_0$  is the electrical resistance before the first washing cycle. Although rGOCY remained black, just as it was coated, after a regular wash, we observed that, when repeatedly washed, rGO particles were removed from the yarn and precipitated in the water. As a result, the unprotected areas of the cotton fiber increased, and the conductivity of the cotton yarn decreased, as illustrated in Figure 8B. As observed, up to the tenth washing cycle, there was only a 40% increase in resistance. From the tenth washing cycle onwards, there was a significant increase in electrical resistance (120%) of the rGOCY. This deterioration was more pronounced compared to what was reported in previous studies<sup>14,46</sup> but significantly less severe than in other works<sup>13</sup>. This analysis provides valuable insights into the durability of rGOCY concerning washing, especially relevant for applications requiring stable electrical properties over time.

### 3.6. Electrical response to relative humidity

The current-voltage (I-V) characteristic curves obtained for a sample rGOCY at different levels of relative humidity are presented in Figure 9A. Linear responses indicate that the continuous conductive network formed by the contact between rGO and cotton along the yarn demonstrates ohmic behavior. It was observed that the different slopes of the lines for various relative humidity levels while maintaining a constant room temperature of 24°C, indicate a strong correlation between the electrical resistance of the yarns and relative humidity. The resistance of the yarn can be calculated as the inverse of the angular coefficient of the I-V curve equation (for ohmic conductors). From the slopes obtained from the I-V graph, it is possible to create a graph that relates resistance to relative humidity, as represented in Figure 9B. Relative air humidity and the rGOCY electrical resistance exhibit correlation coefficients greater than 0.98, confirming a strong linear relationship.

This behavior was previously reported for GO<sup>16</sup> and rGO<sup>47</sup>, indicating that water absorption results in an increase in the electrical resistance in both materials. These results indicate that rGOCY is moisture sensitive. Furthermore, it was noted that the variations are proportional to the same changes in relative humidity, regardless of the initial resistance value ( $R_0$ ) and the characteristics of the yarn. To analyze these variations, the concept of normalized sensitivity ( $S$ ) was adopted, and defined as the ratio of the current resistance at relative humidity levels ( $R$ ) to the initial resistance ( $R_0$ ) expressed in the Equation 4:

$$S = \frac{R}{R_0} \quad (4)$$

Normalized sensitivity ( $S$ ) follows a linear behavior, with angular and linear coefficients varying very little for a given  $R_0$ . In our experiments, we chose the initial state of the sensors to be at 11% relative humidity. Figure 9C presents a swarm chart for the normalized sensitivity of 150 samples of rGOCY about relative humidity. As can be seen, the resistance of all samples increased proportionally with the increase in RH. This means that by adopting a reference relative humidity ( $RH_0$ ), the variation in sensitivity ( $S$ ) is the same, regardless of the initial  $R_0$  resistance of the yarn (whether it is long, short, stretched, or bent) at the  $RH_0$  reference humidity. Figure 9D presents the linear regression between the average values of sensitivities ( $S$ ) from Figure 9C and their respective relative humidities in the range of 11%–90% RH. The Regression coefficient  $R^2$  is 0.993, suggesting that the sensor has good linearity.

Considering that the response  $S$  of all coated yarns is linear and tends to have the same values for angular ( $\alpha$ ) and linear ( $\beta$ ) coefficients, we can establish the general equation:

$$S = \alpha x + \beta \quad (5)$$

Where  $x$  represents relative humidity,  $\alpha = 0.0046$ , and  $\beta = 0.9398$ . By equating Equations 4 and 5, we obtain:

$$\frac{R}{R_0} = \alpha x + \beta \quad (6)$$

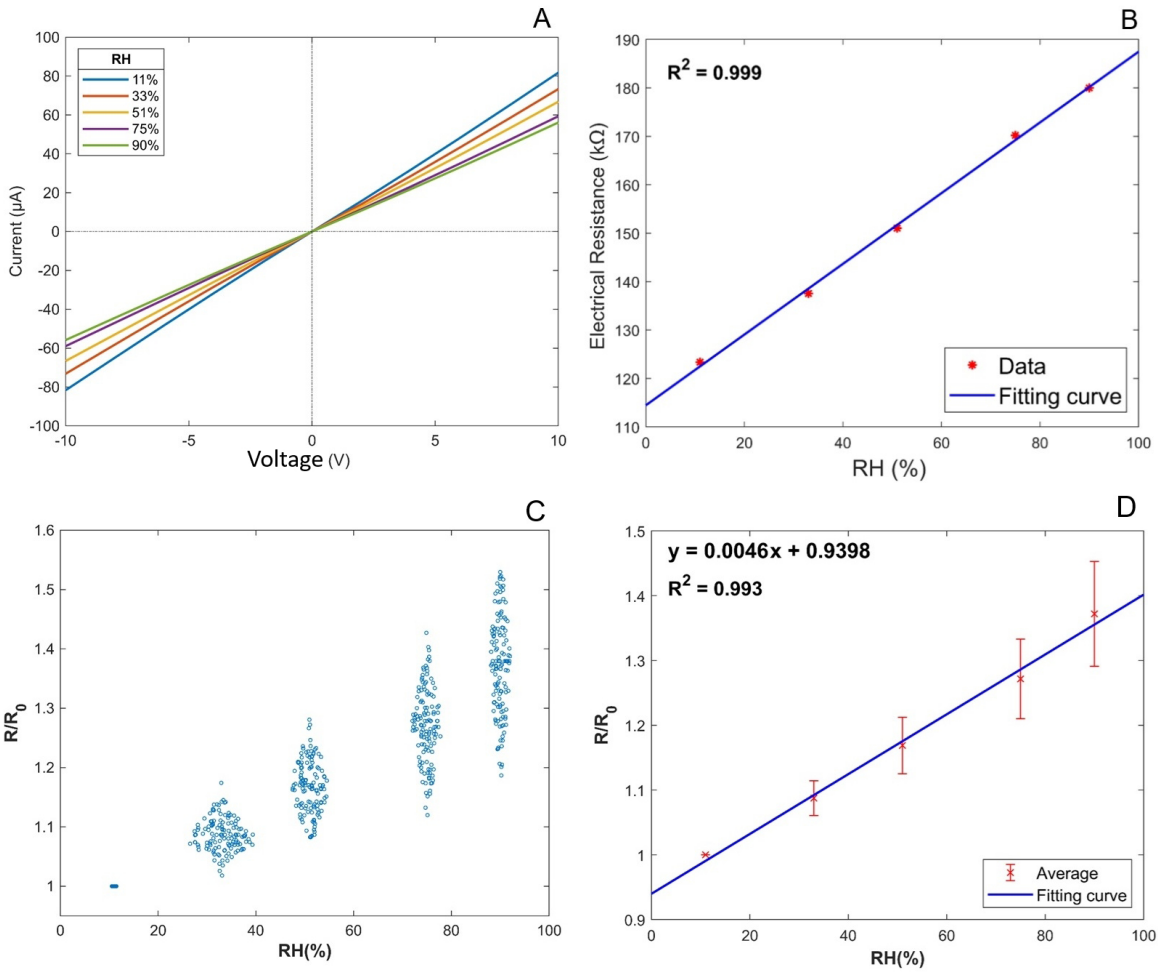


**Figure 9.** (A) I-V curve characteristics of rGOCY for different relative humidity; (B) Resistance versus Relative Humidity curve of rGOCY; (C) normalized sensitivity of 150 rGOCYs samples with respect to relative humidity; (D) linear regression of average sensitivity values (S) from 150 samples as a function of their respective relative humidities.

Isolating  $x$ , we obtain the following equation for relative humidity as a function of the resistance of the wire coated with the nanocomposite, calibrated from an initial relative humidity  $RH_0$  (in this case, 11%), from which we can extract the value of resistance  $R_0$ :

$$x = \frac{1}{\alpha} \left( \frac{R}{R_0} - \beta \right) \quad (7)$$

This calibration methodology is essential as it eliminates the need to perform calibration curves at various humidities. All yarns behave the same way, requiring only knowledge of the yarn's resistance at a specific humidity (in this case, 11%).

### 3.7. Humidity sensing model and calibration

Relative humidity is defined as the ratio between the vapor pressure of water present and the vapor pressure of water required for saturation at a specific temperature. The presence of water vapor in the air is natural, and the relative humidity of the air-water vapor mixture is determined by the relationship between the mass of water vapor in a unit

volume and the mass of water vapor that the volume could contain if it were saturated at the mixture's temperature<sup>48</sup>. Relative humidity is typically expressed as:

$$RH = \frac{P_w}{P_s} \times 100\% \quad (8)$$

where  $P_w$  and  $P_s$  represent the vapor pressure of water and the saturation vapor pressure, respectively. Therefore, the relative humidity of the air does not have negative values and does not exceed 100%.

The equation for relative humidity as a function of the normalized sensitivity of rGOCY (Equation 7), obtained experimentally, is reliable only in the range of 10% to 90% relative humidity. This is due to the inherent statistical variations in the process. Very low relative humidities can result in negative values when using Equation 7, whereas very high relative humidities can yield values above 100% with the same equation. This limitation should be considered when interpreting the results and using the equation in practical applications.

To test the humidity detection performance using rGOCY and ensure that the results of relative humidity (RH) as a function of sensitivity (S) remain between 0 and 100%, we performed the adjustment of Equation 7 using the nonlinear Richard growth model<sup>49</sup> through computational methods. This adjustment was made to make the equation exhibit a sigmoidal function behavior. For relative humidities below 11%, sensitivity decreases asymptotically; for relative humidities between 11% and 90%, sensitivity follows a linear behavior; and for relative humidities above 90%, sensitivity increases asymptotically, as illustrated in Figure 10. The equation of the nonlinear Richard growth model, which provided the best fit in the humidity range between 10% and 90% with an average error of 0.18% compared to Equation 7, is as follows:

$$RH = \frac{100}{\left(1 + 47155e^{-9.4360 \frac{R}{R_0}}\right)^{1.2152}} \quad (9)$$

### 3.8. Relative humidity response tests

Figure 11 displays dynamic curves representing the responses of three types of sensors: a commercial humidity sensor, a sensor with rGOCY without optimization (linear fit), and an optimized rGOCY sensor (nonlinear fit). These responses were recorded concerning variations in relative humidity inside the gas chamber. It can be observed that the response of the rGOCY sensor closely tracks the response of the commercial humidity sensor during cycles of increasing and decreasing internal humidity in the gas chamber. Furthermore, by optimizing the response using the nonlinear Richard growth model, it is evident that the optimized response aligns even more closely with the commercial sensor's response. This result suggests that the optimized response more accurately portrays the behavior of the rGOCY as a humidity sensor. This conclusion is validated when compared to the widely calibrated and used commercial sensor for measuring relative humidity in the air.

This observation highlights the effectiveness of the optimization approach, demonstrating a higher agreement between the data from the optimized rGOCY sensor and the reference measurements from the commercial sensor. This consistency reinforces the potential applicability of the optimized sensor for practical humidity detection applications, with performance closer to that of established sensors.

### 3.9. Dynamic response to relative humidity

Changes in the continuous electrical resistance of rGOCY in response to relative humidity in the gas chamber were monitored to understand the detection kinetics. Figure 12A displays the dynamic response and recovery curve of the rGOCY to variations in relative humidity from 5% to 95% in a gas chamber, while maintaining room temperature. Over 57 seconds, the rGOCY exhibited a positive exponential response to increasing humidity. The response was instantaneous after 20 seconds of exposure to dry air, followed by a transition to a steady state, indicating moisture absorption saturation at a response magnitude of 1.25.

According to the curve, the response and recovery time of the rGOCY, for relative humidity ranging from 5% to 95%, was 57 and 58 seconds, respectively. Data from previous reports on humidity sensing using graphene indicate prolonged response and recovery times, typically around 180 seconds<sup>50</sup>. Repeatability is addressed in Figure 12B, which shows the measured electrical resistance of rGOCY plotted against relative humidity, controlled by saturated solutions at a constant temperature of 24°C. These data represent ten cycles of relative humidity varied in cycles from 6% to 97% (and vice versa) every 10 hours. When humid air was alternated with dry air, rGOCY demonstrated good recoverability characteristics, with the response returning to the initial value.

In Figure 12C, the electrical resistance of rGOCY under bending conditions is measured and shows a slight increase compared to that in the stretched condition within a humidity range of 11–90% RH. According to Ni and coworkers<sup>51</sup>, this phenomenon can be explained as follows: when rGO is coated onto the flexible yarn, the rGO nanosheets partially overlap, as illustrated in Figure 6C. Under stretched conditions, numerous water molecules are adsorbed on defects and remaining hydrophilic groups of rGO, thereby enhancing the output performance of rGOCY.

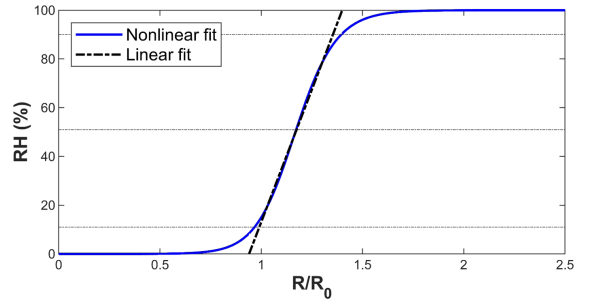


**Figure 10.** Nonlinear growth model for relative humidity (RH) calibration.

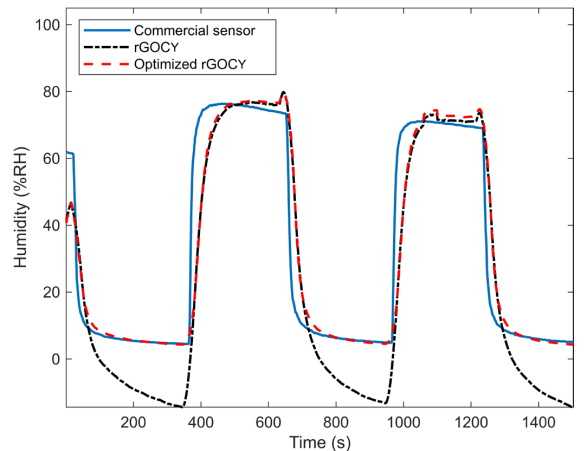


**Figure 11.** Dynamic response comparison among different humidity sensors.

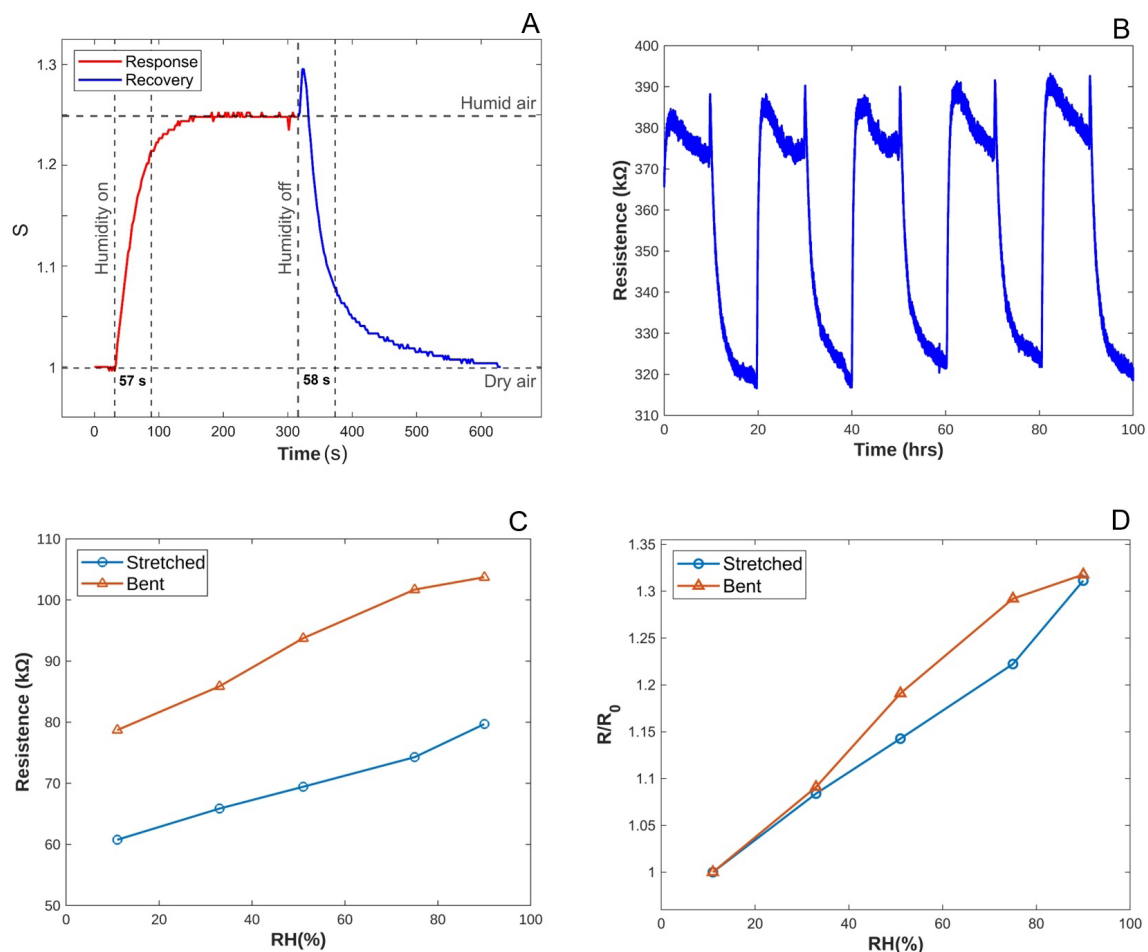


**Figure 12.** (A) Dynamic response of rGO CY to relative humidity changes; (B) resistance versus relative humidity (%RH) with relative humidity varied in cycles; (C) the electrical changes of rGO CY as a function of relative humidity under stretch and bent condition; (D) normalized sensitivity changes of rGO CY as a function of relative humidity under stretch and bent condition.

However, when rGO CY is bent, the overlap between different rGO nanosheets decreases. As a result, rGO CY has a larger surface area and can adsorb more water molecules, leading to a slight increase in its electrical resistance. Fortunately, the reduction in overlap between rGO nanosheets induced by bending has a limited impact on the normalized sensitivity of rGO CY (Figure 12D), demonstrating that the normalized sensitivity remains consistent regardless of the initial electrical resistance. The combination of these features suggests rGO CY's potential for humidity detection and monitoring applications.

#### 4. Conclusions

The investigation into cotton yarn coated with reduced graphene oxide (rGO CY) has revealed its remarkable potential as a versatile material for humidity-sensing applications. Through a series of experiments, we have elucidated crucial aspects of its electrical properties and sensing performance. Specifically, the rGO CY exhibited impressive electrical properties with a specific resistance ( $R_m$ ) of  $80 \pm 7 \Omega \cdot g/cm^2$

after five dip-coating cycles, surpassing prior reported data. This enhanced conductivity, coupled with its linear resistance response, ensures uniform coating along the yarn length, making it a promising candidate for various electronic applications.

Furthermore, our study demonstrated that the sensitivity of the rGO CY to humidity levels remained consistent after only two dip-coating cycles, offering an efficient and reliable humidity-sensing solution. Importantly, we determined that the optimal number of dip-coating cycles for this application is three, resulting in mass-specific resistance ( $120.3 \Omega \cdot g/cm^2$ ), linear resistance ( $84.7 k\Omega/cm$ ), and a highly linear response ( $R^2 = 0.98$ ) between electrical resistance and relative humidity. Moreover, the rGO CY exhibited excellent mechanical flexibility and durability, showcasing its potential for use in flexible electronic devices.

As an additional advantage, we have shown that the use of chicken egg albumin (CEA) as a binder for rGO outperforms the conventionally used binding agents. CEA not only provides strong binding properties but also maintains the yarn's electrical stability, even after multiple washing cycles.

This advantage ensures the long-term reliability of rGOCY in practical applications. Overall, this study highlights the immense promise of rGOCY as a humidity sensor, emphasizing its exceptional electrical properties, mechanical flexibility, and the advantage of employing CEA over other binding agents. These findings open up exciting possibilities for the utilization of rGOCY in diverse fields, from wearable electronics to environmental monitoring, where precise and robust humidity sensing is essential.

## 5. Acknowledgements

The authors were grateful for the financial support from FACEPE (grant n. IBPG-0480-3.09/20), CNPq, CAPES, as well as Central Multiusuário DF/UFPE, LARNano/DEN/UFPE.

## 6. References

- Jang HS, Moon MS, Kim BH. Electronic textiles fabricated with graphene oxide-coated commercial textiles. *Coatings*. 2021;11(5):489.
- Kinloch IA, Suhr J, Lou J, Young RJ, Ajayan PM. Composites with carbon nanotubes and graphene: an outlook. *Science*. 2018;362(6414):547-53.
- Bolotin KI, Sikes KJ, Jiang Z, Klima M, Fudenberg G, Hone J, et al. Ultrahigh electron mobility in suspended graphene. *Solid State Commun*. 2008;146(9-10):351-5.
- Balandin AA, Ghosh S, Bao W, Calizo I, Teweldebrhan D, Miao F, et al. Superior thermal conductivity of single-layer graphene. *Nano Lett*. 2008;8(3):902-7.
- Stoller MD, Park S, Zhu Y, An J, Ruoff RS. Graphene-based ultracapacitors. *Nano Lett*. 2008;8(10):3498-502.
- Koçanalı A, Apaydın Varol E. An experimental study on the electrical and thermal performance of reduced graphene oxide coated cotton fabric. *Int J Energy Res*. 2021;45(9):12915-27.
- Liu Q, Zhang Y, Li A, Ren E, Cui C, Zhou M, et al. Reduced graphene oxide-coated carbonized cotton fabric wearable strain sensors with ultraloud detection limit. *J Mater Sci Mater Electron*. 2020;31(20):17233-48.
- Karimi L, Yazdanshenas ME, Khajavi R, Rashidi A, Mirjalili M. Using graphene/TiO<sub>2</sub> nanocomposite as a new route for preparation of electroconductive, self-cleaning, antibacterial and antifungal cotton fabric without toxicity. *Cellulose*. 2014;21(5):3813-27.
- Ghosh S, Ganguly S, Das P, Das TK, Bose M, Singha NK, et al. Fabrication of reduced graphene oxide/silver nanoparticles decorated conductive cotton fabric for high performing electromagnetic interference shielding and antibacterial application. *Fibers Polym*. 2019;20(6):1161-71.
- Kim E, Arul NS, Han JI. Electrical properties of conductive cotton yarn coated with eosin y functionalized reduced graphene oxide. *J Nanosci Nanotechnol*. 2016;16(6):6061-7.
- Park JJ, Hyun WJ, Mun SC, Park YT, Park OO. Highly stretchable and wearable graphene strain sensors with controllable sensitivity for human motion monitoring. *ACS Appl Mater Interfaces*. 2015;7(11):6317-24.
- Yaghoubidoust F, Salimi E, Wicaksono DHB, Nur H. Physical and electrochemical appraisal of cotton textile modified with polypyrrole and graphene/reduced graphene oxide for flexible electrode. *J Textil Inst*. 2021;112(4):646-58.
- Bhattacharjee S, Macintyre CR, Wen X, Bahl P, Kumar U, Chughtai AA, et al. Nanoparticles incorporated graphene-based durable cotton fabrics. *Carbon*. 2020;166:148-63.
- Yun YJ, Hong WG, Kim WJ, Jun Y, Kim BH. A novel method for applying reduced graphene oxide directly to electronic textiles from yarns to fabrics. *Adv Mater*. 2013;25(40):5701-5.
- Yun YJ, Hong WG, Choi NJ, Kim BH, Jun Y, Lee HK. Ultrasensitive and highly selective graphene-based single yarn for use in wearable gas sensor. *Sci Rep*. 2015;5:10904.
- Wang Y, Zhang L, Zhang Z, Sun P, Chen H. High-sensitivity wearable and flexible humidity sensor based on graphene oxide/non-woven fabric for respiration monitoring. *langmuir*. 2020;36(32):9443-8.
- Jingru S, Yong X. Separation and purification of bovine serum albumin by non-organic solvent liquid-solid extraction system. In: 2007 1st International Conference on Bioinformatics and Biomedical Engineering; 2007; Wuhan, China. Proceedings. New York: IEEE; 2007. p. 72-5.
- Shiomori K, Ebuchi N, Kawano Y, Kuboi R, Komasa I. Extraction characteristic of bovine serum albumin using sodium bis(2-ethylhexyl) sulfosuccinate reverse micelles. *J Ferment Bioeng*. 1998;86(6):581-7.
- Tanaka K, Sawatani E, Shigueoka EM, Dias GA, Nakao HC, Arashiro F. Isolation of bovine plasma albumin by liquid chromatography and its polymerization for use in immunohematology. *Braz J Med Biol Res*. 2001;34(8):977-83.
- Chang JW, Wang CG, Huang CY, Tsai TD, Guo TF, Wen TC. Chicken albumen dielectrics in organic field-effect transistors. *Adv Mater*. 2011;23(35):4077-81.
- Bok CH, Woo SJ, Wu C, Park JH, Kim TW. Flexible bio-memristive devices based on chicken egg albumen: Au@SiO<sub>2</sub> core-shell nanoparticle nanocomposites. *Sci Rep*. 2017;7(1):12033.
- Lv C, Hu C, Luo J, Liu S, Qiao Y, Zhang Z, et al. Recent advances in graphene-based humidity sensors. *Nanomaterials*. 2019;9(3):422.
- Hummers WS Jr, Offeman RE. Preparation of graphitic oxide. *J Am Chem Soc*. 1958;80(6):1339.
- Oliveira AEF, Braga GB, Tarley CRT, Pereira AC. Thermally reduced graphene oxide: synthesis, studies and characterization. *J Mater Sci*. 2018;53(17):12005-15.
- Guérin-Dubiard C, Audic JJ. Egg-protein-based films and coatings. In: Huopalahti R, López-Fandiño R, Anton M, Schade R, editors. Bioactive egg compounds. Berlin: Springer; 2007. p. 265-73.
- Li Z, Huang X, Tang Q, Ma M, Jin Y, Sheng L. Functional properties and extraction techniques of chicken egg white proteins. *Foods*. 2022;11(16):2434.
- An W, Ma J, Xu Q, Fan Q. Flame retardant, antistatic cotton fabrics crafted by layer-by-layer assembly. *Cellulose*. 2020;27(14):8457-69.
- Morton WE, Hearle JWS. Physical properties of textile fibers. 3rd ed. London: Textile Institute; 1993.
- Carr DS, Harris BL. Solutions for maintaining constant relative humidity. *Ind Eng Chem*. 1949;41(9):2014-5.
- Ju HM, Huh SH, Choi SH, Lee HL. Structures of thermally and chemically reduced graphene. *Mater Lett*. 2010;64(3):357-60.
- Emiru TF, Ayele DW. Controlled synthesis, characterization and reduction of graphene oxide: a convenient method for large scale production. *Egypt J Basic Appl Sci*. 2017;4(1):74-9.
- Galpaya D, Wang M, George G, Motta N, Waclawik E, Yan C. Preparation of graphene oxide/epoxy nanocomposites with significantly improved mechanical properties. *J Appl Phys*. 2014;116(5):053518.
- Marcano DC, Kosynkin DV, Berlin JM, Sinitskii A, Sun Z, Slesarev A, et al. Improved Synthesis of Graphene Oxide. *ACS Nano*. 2010;4(8):4806-14.
- Stankovich S, Piner RD, Nguyen ST, Ruoff RS. Synthesis and exfoliation of isocyanate-treated graphene oxide nanoplatelets. *Carbon*. 2006;44(15):3342-7.
- Lataste JF. Electrical resistivity for the evaluation of reinforced concrete structures. In: Maierhofer C, Reinhardt HW, Dobmann G, editors. Non-destructive evaluation of reinforced concrete structures. Boca Raton: CRC Press; 2010. p. 243-75.
- Kasaw E, Haile A, Getnet M. Conductive coatings of cotton fabric consisting of carbonized charcoal for e-textile. *Coatings*. 2020;10(6):579.

37. Liu Y, Li Z, Feng Y, Yao J. Scale production of conductive cotton yarns by sizing process and its conductive mechanism. *SN Appl Sci.* 2021;3(6):611.
38. Xu J, Wang D, Yuan Y, Wei W, Duan L, Wang L, et al. Polypyrrole/reduced graphene oxide coated fabric electrodes for supercapacitor application. *Org Electron.* 2015;24:153-9.
39. Li W, Chen R, Qi W, Cai L, Sun Y, Sun M, et al. Reduced graphene oxide/mesoporous ZnO NSs hybrid fibers for flexible, stretchable, twisted, and wearable NO<sub>2</sub> e-textile gas sensor. *ACS Sens.* 2019;4(10):2809-18.
40. Wu R, Ma L, Patil A, Meng Z, Liu S, Hou C, et al. Graphene decorated carbonized cellulose fabric for physiological signal monitoring and energy harvesting. *J Mater. J Mater Chem A Mater Energy Sustain.* 2020;8(25):12665-73.
41. Yun YJ, Ah CS, Hong WG, Kim HJ, Shin JH, Jun Y. Highly conductive and environmentally stable gold/graphene yarns for flexible and wearable electronics. *Nanoscale.* 2017;9(32):11439-45.
42. Yun YJ, Lee HJ, Son TH, Son H, Jun Y. Mercerization to enhance flexibility and electromechanical stability of reduced graphene oxide cotton yarns. *Compos Sci Technol.* 2019;184:107845.
43. Mizerska U, Fortuniak W, Makowski T, Svyntkivska M, Piorkowska E, Kowalczyk D, et al. Antibacterial electroconductive rGO modified cotton fabric. *Polym Adv Technol.* 2021;32(10):3975-81.
44. Xu LL, Guo MX, Liu S, Bian SW. Graphene/cotton composite fabrics as flexible electrode materials for electrochemical capacitors. *RSC Adv.* 2015;5(32):25244-9.
45. Cai G, Xu Z, Yang M, Tang B, Wang X. Functionalization of cotton fabrics through thermal reduction of graphene oxide. *Appl Surf Sci.* 2017;393:441-8.
46. Kang MA, Ji S, Kim S, Park CY, Myung S, Song W, et al. Highly sensitive and wearable gas sensors consisting of chemically functionalized graphene oxide assembled on cotton yarn. *RSC Adv.* 2018;8(22):11991-6.
47. Jiang W, Zhang F, Lin Q. Flexible relative humidity sensor based on reduced graphene oxide and interdigital electrode for smart home. *Micro & Nano Lett.* 2022;17(6):134-8.
48. Lee CY, Lee GB. Humidity sensors: a review. *Sens Lett.* 2005;3(1):1-15.
49. Richards FJ. A Flexible growth function for empirical use. *J Exp Bot.* 1959;10(2):290-301.
50. Ghosh A, Late DJ, Panchakarla LS, Govindaraj A, Rao CNR. NO<sub>2</sub> and humidity sensing characteristics of few-layer graphenes. *J Exp Nanosci.* 2009;4(4):313-22.
51. Ni L, Li X, Cai F, Dong Z, Deng Y, Jiang T, et al. Printable and flexible humidity sensor based on graphene -oxide-supported MoTe<sub>2</sub> nanosheets for multifunctional applications. *Nanomaterials.* 2023;13(8):1309.